J Supercond Nov Magn (2017) 30:931–936
DOI 10.1007/s10948-016-3885-4

ORIGINAL PAPER

Particularities of the Magnetic State of CuO Nanoparticles Produced by Low-Pressure Plasma Arc Discharge

A. A. Lepeshev[1,2] · I. V. Karpov[1,2] · A. V. Ushakov[1,2] · D. A. Balaev[2,3] · A. A. Krasikov[3] · A. A. Dubrovskiy[3] · D. A. Velikanov[3] · M. I. Petrov[1,3]

Received: 2 August 2016 / Accepted: 27 October 2016 / Published online: 7 November 2016
© Springer Science+Business Media New York 2016

Abstract Copper oxide nanoparticles were produced by direct plasmachemical synthesis in a plasma arc discharge of low pressure. The formation of CuO nanoparticles with an average size of 12 nm and narrow size distribution intervals was determined by using the x-ray diffraction analysis and TEM microscopy methods. It was defined by using a vibration magnetometer and a SQUID magnetometer, that the magnetic properties of CuO nanoparticles with such size were extremely different from the magnetic properties of bulk antiferromagnetic CuO. Structural defects caused the formation of a ferromagnetic state, remaining at least up to the room temperature. The temperature of corresponding antiferromagnetic ordering was significantly decreased (down to ∼ 100 K). Meanwhile, some of the copper surface spins showed a spin-glass behavior at low temperatures.

Keywords CuO nanoparticles · Plasmachemical synthesis · Magnetic properties · Vibration magnetometer

1 Introduction

Over the last few decades, the magnetism of nanodispersed systems was one of the highest priority areas of investigation due to a large number of industrial applications, especially the priority of the explanation of some properties of bulk materials [1]. The magnetic properties of nanoparticles were determined primarily by the surface distribution of spins opposite to macroparticles. For example, nanoparticles of the antiferromagnetic material in its bulk form, obtain magnetic moments, described in [2]. Its appearance, predicted by Néel [3], is caused by definite structural defects and surface effects. This fact opens prospects for new practical applications of antiferromagnetic (AF) nanoparticles [4, 5]. On the other hand, decreasing the particle size causes changing the parameters which characterize their magnetic state (anisotropy, Néel temperature TN), and it is also a reason for further investigations [4–12].

Copper oxide, which will be discussed in this paper, is an antiferromagnetic material with the value of T_N ≈230 K [4, 5, 13–17]; however, in the temperature range over T_N (550 K) spin correlations remain to be the same and it is caused by quasi-one-dimensional antiferromagnetism. This feature distinguishes CuO from other relatively well-studied systems of AF nanoparticles, such as NiO [2, 18], Fe_2O_3, [19] for their magnetic behavior is described in detail based on various classical approaches applied to magnetic nanoparticles (superparamagnetic behavior, blocking processes).

Copper oxide nanoparticles are generally synthesized by wet chemical processes [20–22]. However, it is difficult to provide the homogeneity and crystallinity of the nanoparticles being produced using these methods. This is because wet chemical processes imply low temperatures. In contrast to wet chemical processes, thermal plasma-based processes imply the evaporation of the component metals at temperatures higher than 10,000 K, followed by rapid condensation gas phases [23–27]. Thermal plasma-based processes have other advantages in comparison with wet

---

✉ A. A. Lepeshev
sfu-unesco@mail.ru

1 Krasnoyarsk Scientific Center of the Siberian Branch, Russian Academy of Science Krasnoyarsk, Russia

2 Siberian Federal University, Krasnoyarsk, 660074, Russia

2 L.V. Kirensky Institute of Physics, Krasnoyarsk, 660036, Russia

chemical processes. One of the advantages is that using these processes, it is possible to prevent impurities addition to the end products; the case does not refer to wet chemical processes. According to such processes, a number of thermal plasma processes have been developed. The vacuum arc plasma evaporation (VAPE) method is commonly used in the processes for the deposition of thin films and the production of nanoparticles [28–33].

This paper represents the results of studying the morphology, the phase composition, and the magnetic state of CuO nanoparticles produced in the low-pressure arc discharge. A specific objective of this study is to define the cause, which leads to an increase of the intragranular critical current (and additional strengthening the Abrikosov vortices pinning) in composite materials made of YBa_2CuO_7 high temperature superconductor and CuO nanoparticles produced by this method [34–36].

2 Experimental

The synthesis of CuO nanopowder was performed in a plasma-chemical reactor, described in detail in [37]. The arc evaporator, used in the process, had the following characteristics: a current arc of 100 A, an intensity of the longitudinal magnetic field excited by a focusing coil on the surface of the cathode, of 80 A/m, with a distance between the cathode and the anode of $d = 50$ mm. A rod, made of high-purity copper (99.99 %) with a diameter of 80 mm and a length of 100 mm, was used as a sputtering cathode. It was placed on a water-cooled copper current lead. In order to begin plasma chemical reactions, the chamber gas was preliminary pumped out to a pressure of $p = 1$ mPa and then it was filled by a gas mixture containing 40 vol. % O_2 from N_2 plasma-generating gas in the input. To study the pressure influence, nanoparticles were synthesized at a basic pressure of 80 Pa. Oxygen was supplied to the reactor in order to form a uniform layer around the plasma torch. The reaction products were collected during 10 min on a hemispherical collector made of water-cooled stainless steel, placed at a distance of 0.12 m from the cathode. Table 1 describes the operating parameters of the reactor during the synthesis.

The morphological composition of the samples was studied by transmission electron microscope JEOL JEM-2100. Studying the phase composition of the samples was carried out using Advance D8 x-ray diffractometer in CuKα monochromatic radiation. Scanning was performed at room temperature in the range of angles at 30–70° with 2θ step of 0.06°. The microstructural characteristics and the elementary cell pa rameters were determined using x-ray full-profile analysis by using the Rietveld method [38].

The magnetic properties were investigated by means of a vibration magnetometer and a SQUID magnetometer. The magnetization curves ($M(H)$ dependences) were measured after passing the cooling conditions in a zero magnetic field (zero field cooled, ZFC). The temperature correlations of the magnetic moment $M(T)$ were measured under ZFC conditions as well as after cooling in an external field (field cooled, FC).

Table 1 Operating parameters of a vacuum plasma-chemical reactor for CuO synthesis

Parameter	Regimes
Basic pressure in chamber	10^{-3} Pa
Arc discharge current	100 A
Voltage	70 V
Power	10 kW
Supply of plasma-forming gas (nitrogen)	60 Pa
Supply of reaction gas (oxygen)	40 vol.% O_2

3 Results and Discussion

Figure 1 shows the TEM images, histogram, and probability density functions of nanosized copper oxide nanoparticles produced at the pressure of the gas mixture (40 vol. % O_2 + 60 % N_2) of 80 Pa.

It is obvious from the results above that the produced powder represents strongly agglomerated particles of a spherical shape. The particle size ranges from 5 to 20 nm. The combination of normal and log-normal size distributions characterizes these particles. This suggests two competing mechanisms of particle condensation from a steam-plasma phase: cluster and steam condensations. The mixed density function under study represents the sum of the density functions of lognormal and normal distribution with adjustable parameters. It is obvious from the figure above that this function describes the particle size distribution much better. The average particle size was 12.4 nm, the mean mass particle size was 13.2 nm, and the standard deviation was 1.18.

Nanopowders are characterized by a high surface energy, which is compensated by a significant aggregation of powders, and this process causes a significant decrease of the specific surface. Since the nanoparticle synthesis in a plasmachemical reactor is always accompanied by definite chemical processes, the size distribution function of nanoparticles becomes more complicated because of the products of these reactions. The morphology of the particles also becomes more complicated and various particles of different chemical composition are formed. Besides, interdiffusion of nanoparticles in the condensed phase occurs. Under a sufficiently high temperature, multiple processes can occur simultaneously, forming strong coupling between

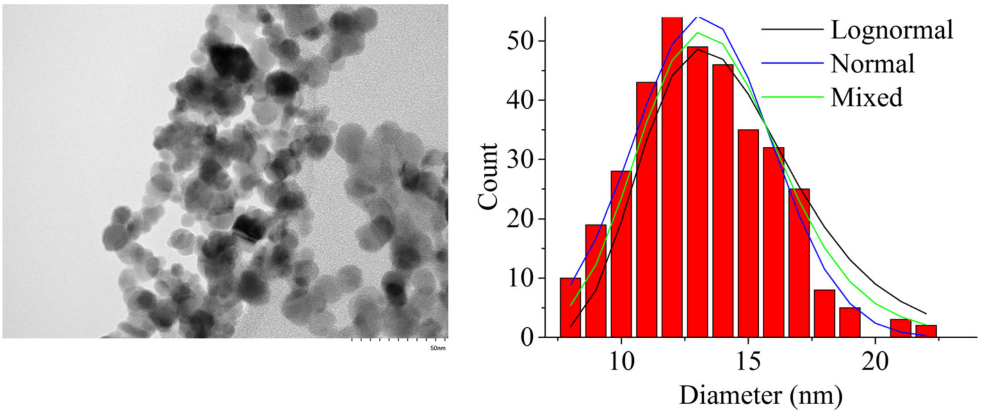

Fig. 1 TEM images, histogram, and probability density functions of nanosized copper oxide powders produced under the pressure of the gas mixture (40 vol. % $O_2 + 60$ % N_2) equal to 80 Pa

the nanoparticles. The experimental data are described by a normal distribution while prevailing nanoparticles layered growth due to the adsorption of atoms and the diffusion processes during corresponding atomic mass transfer at the interface.

Figure 2 shows the x-ray diffraction pattern of nanoparticles, synthesized under the pressure of the gas mixture (40 vol. % $O_2 + 60$ % N_2) for the values of 2θ in the range from 30° to 70°.

The XRD pattern clearly illustrates that the copper oxide nanoparticles, formed during the synthesis, have a crystalline nature, and monoclinic crystal structure of CuO (PDF 4+ #00-045-0937) with lattice parameters of $a = 4.691$ Å, $b = 3.432$ Å, and $c = 5.138$ Å.

Figure 3 shows the temperature dependences of the magnetic moment $M(T)$ in various applied magnetic fields and a definite thermal magnetic prehistory (ZFC and FC).

The following facts are of a special interest. Firstly, there is a strong influence of thermomagnetic prehistory on the type of the $M(T)$ curve shown in the graph, moreover, in a stronger field ($H = 5$ kOe) the manifestation of the effect is less. Secondly, increasing the applied field causes radical changes of the temperature behavior of the $M(T)$ curve, as illustrated by Fig. 4.

This behavior of CuO nanoparticles is fundamentally different from the properties of their "bulk analogue"—polycrystalline CuO [5–7, 10–14], for which the $M(T)$ curve in the field of $H = 1$ kOe is shown in Fig. 4. It shows independence of the magnetic susceptibility (or M/H value) from the magnetic field and its increase is correlated with an increase of the temperature, with the maximum of the derivative dM/dT in the vicinity of TN, and then it demonstrates a plateau in the range of 300–550 K [12, 13]. It should be noted that the values of the magnetic moment for the CuO nanoparticles exceeds the value of the magnetic susceptibility of polycrystalline CuO (in the field of $H = 1$ kOe almost by one order).

The mentioned differences in the magnetic behavior of CuO nanoparticles appear in this type of the dependences of $M(H)$ as well, as shown in Fig. 5.

At $T = 4.2$ K, the $M(H)$ curves show a hysteresis with the coercive force of approximately 0.5 kOe (Fig. 5, inset).

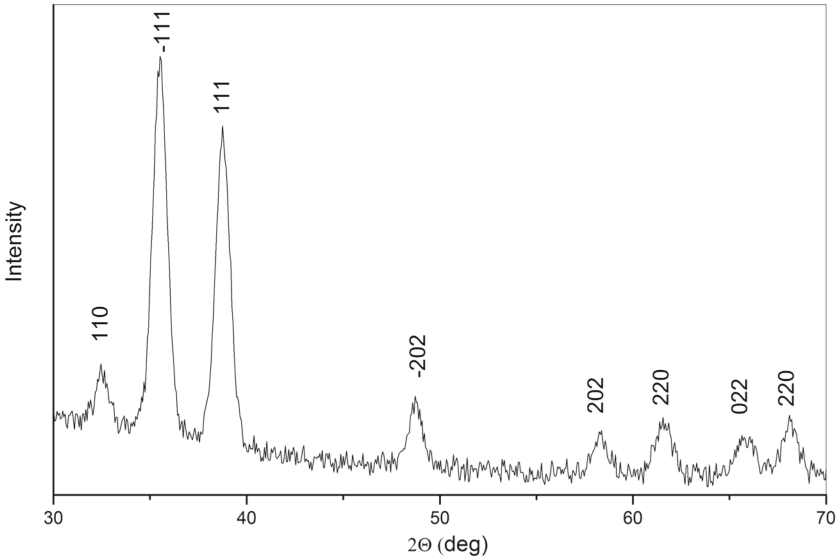

Fig. 2 XRD pattern of copper oxide nanopowder produced under the pressure of the gas mixture (40 vol. % $O_2 + 60$ % N_2) equal to 80 Pa

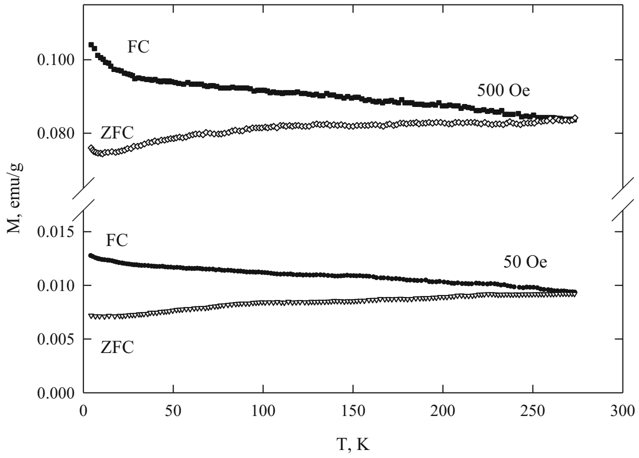

Fig. 3 The temperature dependences of the magnetic moment $M(T)$ of CuO nanoparticles in the external fields of 50 and 500 Oe and various thermomagnetic prehistory

At the temperatures of 100–250 K, the $M(H)$ curves of CuO nanoparticles are characterized by quite a sharp increase in the range of up to ∼ 10 kOe (Fig. 5, *inset*) and then it demonstrates a plateau. For example, Fig. 5 also shows the dependences of $M(H)$ for polycrystalline CuO at $T = 4.2$ K, which is linear throughout the whole field.

Based on the observed behavior of the magnetic properties of CuO nanoparticles, it can be concluded that the investigated system includes a few magnetic phases. Firstly, it is a ferromagnetic (FM) phase, which exists, at least at room temperatures. Secondly, it is a “paramagnetic” contribution, a sharp difference of $M(H)$ curves for the temperatures of 4.2 and 100 K (Fig. 3) and decreasing character of $M(T)$ curves in the fields of $H = 5$ and 10 kOe (Fig. 4).

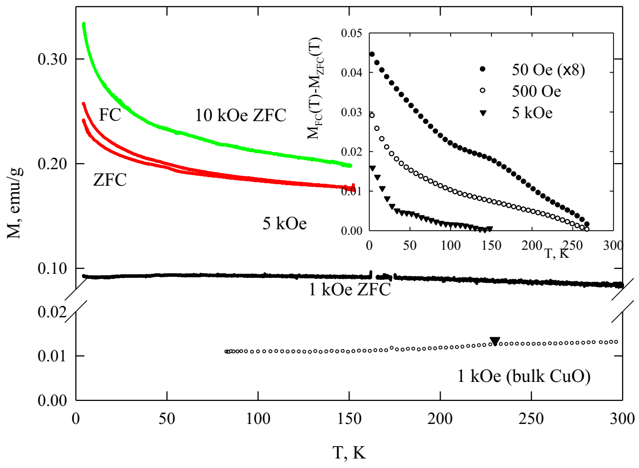

Fig. 4 The temperature dependences $M(T)$ of CuO nanoparticles in various applied fields and ZFC and FC conditions. The data for polycrystalline (bulk CuO) and Néel temperature (230 K) are also shown. *Inset* dependences of $M_{\mathrm{ZFC}}(T)$-$M_{\mathrm{FC}}(T)$ for the external field of 50 and 500 Oe and 5 kOe

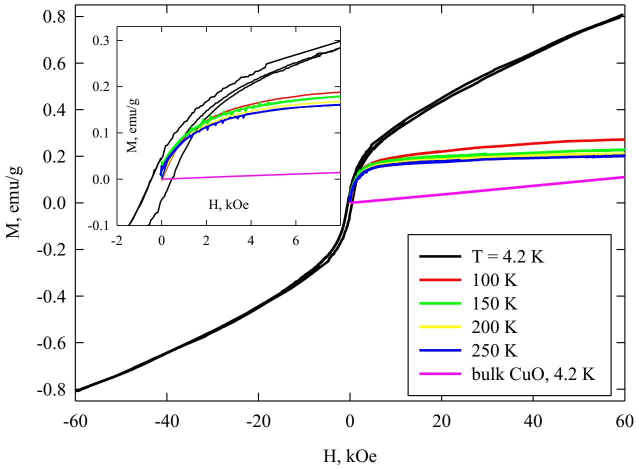

Fig. 5 $M(H)$dependences of CuO nanoparticles under the indicated temperatures. The data for polycrystalline (bulk CuO) is also shown at $T = 4.2$ K. *Inset* fields range of up to 8 kOe within a larger scale

With respect to the antiferromagnetic phase, the investigated CuO nanoparticles do not show peculiar behavior in the vicinity of the point corresponding to 230 K. This reveals, at least, a significant reduction of the Néel temperature for the investigated CuO nanoparticles. The temperature range within AF ordering will be discussed below.

Let us consider the possibility of the appearance of these phases in nanodimensional copper oxide. Taking into account a sufficiently rapid decrease of the magnetic moment, caused by paramagnetic contribution with the temperature growth, it is possible to make an approximate estimation of FM contribution taking into account the magnetization isotherms (Fig. 3). $M_{\mathrm{FM}} \sim 0.2$ emu/g (for low temperatures). At the effective value of the magnetic moment of Cu in CuO equal to ≈0.7 μ_{B} (μ_{B} is a Bohr magneton) [15], it is possible to find that the percentage of FM-ordered atoms is equal to $\sim 4 \times 10^{-3}$ of all copper atoms. Let us note that the experimental data, given in Figs. 1–3, show that the magnetic moments, corresponding to the FM phase, are in locked position.

According to Néel [3], a small AF particle can have uncompensated magnetic moment μ_{FM} due to various defects on the surface (1), in the volume of particle (2), and also due to odd number of ferromagnetic planes (3). Its value depends on the type of defects (1)–(3) and can be estimated by the expression: $\mu_{\mathrm{FM}} \sim \underline{N}^{b} \times \mu$, where N is a number of magnetically active atoms in a particle, μ is a magnetic moment of this atom, and b is an exponent which is equal to 1/3, 1/2, and 2/3 for cases (1), (2), and (3), respectively. A particle of CuO with a size of ∼ 15 nm contains approximately $75^3 \sim 4.2 \times 10^5$ atoms of Cu^{2+}. For the calculated above percentage of FM-ordered moments of copper atoms ($\sim 4 \times 10^{-3}$), it is possible to estimate the amount of

FM-ordered atoms in a 15-nm particle, which is equal to ∼ 1.7 $\times 10^3$. This value is quite close to the Néel hypothesis (3), in which an odd number of FM planes is a reason of FM moment existence: $N^{2/3} \sim 5.6 \times 10^3$ at $N \approx 4.2 \times 10^5$.

It is known that the exchange interaction in the copper monoxide has an order of ∼ 400 K [6, 17], and close ferromagnetic order can be kept up to rather high temperatures. Most probably, this is a reason for the FM contribution observed in CuO particles, at least in the range up to the room temperature.

Let us consider the temperature-dependent paramagnetic contribution. A rapid decrease of the magnetic moment with an increase of the temperature, which is observed for $M(T)$ curves in the fields of $H = 5$ and 10 kOe (Fig. 4), shows a "paraprocess," which can be described by the Brillouin function $B(H, T)$ in the classic case of non-interacting spins. However, for the low temperatures, the evaluation of results showed that $M(T)$ curves in the fields $H = 5$ and 10 kOe vary with temperature changes more slowly than the Brillouin function with a magnetic moment of ≈0.7 μB. This fact, as well as the observed discrepancy between $M(T)$ curves in the fields of $H = 5$ and 10 kOe for different magnetic prehistory, indicates the spin-glass behavior of the spins of this subsystem. On the other hand, a simplified calculation of $M(H)$ dependences at $T = 4.2$ K excluding hysteresis and taking into account only two addends $M_{\mathrm{FM}}(H) \sim$ const ∼ 0.2 emu/g while $M_{\mathrm{PM}} \times B(H)$ allows estimating the value of the discussed paramagnetic contribution, which was equal to $M_{\mathrm{PM}} \sim 1$ emu/g (±20 %). This value corresponds to ∼ 2 % of the total amount of copper atoms, and it is equal to $\sim 9 \times 10^3$ for these 15-nm particle; the value is close to the amount of surface atoms of such a particle ($\sim 30 \times 10^3$) while estimating the order of this value. Thus, a subsystem of surface atoms can be discussed, which exhibit the spin-glass properties at low temperatures, and they can behave as a paramagnetic subsystem at high fields and high temperatures. It should be noted that the paramagnetic behavior of the surface atoms of CuO nanoparticles at temperatures above 80 K was also observed in [13, 14].

Regarding the paramagnetic contribution, dominating at low temperatures, as well as FM subsystem, it is quite difficult to identify the magnetic transition and estimate the Néel temperature for the studied CuO nanoparticles system. $M(T)$ dependences measured in the corresponding ZFC conditions in the weak fields of 50 and 500 Oe, in which the contribution of "paramagnetic phase" is insignificant, show the greatest increase in the temperature range of up to 100 K. It can be assumed that the Néel temperature for these CuO nanoparticles is considerably decreased in comparison with the bulk analogue, and it is equal to the order of about 100 K. Some confirmation of this conclusion is the behavior of the difference $M_{\mathrm{ZFC}}(T)$–$M_{\mathrm{FC}}(T)$, shown in the inset of Fig. 4. Quite a sharp increase of $M_{\mathrm{ZFC}}(T)$–$M_{\mathrm{FC}}(T)$ (within a decrease in temperature) was observed namely at temperatures below 100 K. This fact was proved also in [6] for the vicinity of the Néel temperature. Meanwhile, although the difference in the thermal magnetic prehistory is not typical for the transition to AF state, it should be noted that, the surface spins ("vapor-phase" discussed above) can be partially explained by an "AF-core" phenomenon. To be more precise, the effects of thermomagnetic prehistory greatly manifest during AF ordering of the core. A relatively small decrease in the T_N value (by 10∼) for nanoscale CuO substance correlates with an increase of Cu–Cu distance and therefore with a decrease of the exchange constants values [5]. Strong reducing of Néel temperature (down to 10–100 K) is caused by a size effect (finite-size effect [7]).

4 Conclusion

Thus, based on the analysis of the magnetic data, we can suggest the following simplified model of the magnetic state of CuO nanoparticles produced by plasma arc discharge of low pressure. A "core" of particles has an antiferromagnetic order with a Néel temperature, significantly less than of their bulk analogue ∼ 100 K. The surface copper atoms behave as paramagnetic, or more precisely, as a partial spin-glass subsystem. They can be exchange-coupled with the core of the particles, and with the ferromagnetic constituent, which is caused by the close ferromagnetic order, existing at least up to the room temperatures.

The presence of the ferromagnetic constituent in the studied CuO nanoparticles can be a reason of the observed increase of pinning (fish-tail effect) in composites YBCO + nanoCuO [34].

Acknowledgments The work was performed with a support of the grant of the Russian Science Foundation (project no. 16-19-10054)

References

1. Batlle, X., Labarta, A.: J. Phys. D **35**, R15 (2002). stacks.iop.org/JPhysD/35/R15
2. Mørup, S., Madsen, D.E., Fradsen, C., Bahl, C.R.H., Hansen, M.F.: J. Phys.: Condens. Matter. **19**, 213202 (2007). doi:10.1088/0953-8984/19/21/213202
3. Néel, L.: CR Acad Sciences. Paris **252**, 4075 (1961)
4. Raikher, Y.U.L., Stepanov, V.I.: J. Exp. Theor. Phys. **107**, 435 (2008). doi:10.1134/S1063776108090112
5. Dobretsov, K., Stolyar, S., Lopatin, A.: Acta Otorhinolaryngol Ital **35**, 97 (2015)
6. Punnoose, A., Magnone, H., Seehra, M.S., Bonevich, J.: Phys. Rev. B **64**, 174420 (2001). doi:10.1103/PhysRevB.64.174420
7. Zheng, X.G., Xu, C.N., Nishikubo, K., Nishiyama, K., Higemoto, W., Moon, W.J., Tanaka, E., Otabe, E.S.: Phys. Rev. B **72**, 014464 (2005). doi:10.1103/PhysRevB.72.014464

8. Bianchi, A.E., Stewart, S.J., Zysler, R.D., Punte, G.: J. Appl. Phys. **112**, 083904 (2012). doi:10.1063/1.4758307
9. Golosovsky, I.V., Mirebeau, I., Andre, G., Kurdyukov, D.A., Kumzerov, Y.u.A., Vakhrushev, S.B.: Phys. Rev. Lett. **86**, 5783 (2001). doi:10.1134/S1063783406110151
10. Kumzerov, Y.u.A., Kartenko, N.F., Parfen'eva, L.S., Smirnov, I.A., Sysoeva, A.A., Misiorek, H., Jezowski, A.: Phys. Solid State **54**, 1066 (2012). doi:10.1134/S1063783412050228
11. Thota, S., Shim, J.H., Seehra, M.S.: J. Appl. Phys. **114**, 214307 (2013). doi:10.1063/1.4838915
12. Balaev, D.A., Krasikov, A.A., Dubrovskiy, A.A., Popkov, S.I., Stolyar, S.V., Bayukov, O.A., Iskhakov, R.S., Ladygina, V.P., Yaroslavtsev, R.N.: JMMM **410**, 171 (2016). doi:10.1016/j.jmmm.2016.02.059
13. Arbuzova, T.I., Naumov, S.V., Samokhvalov, A.A., Gizhevskii, B.A., Arbuzov, V.L., Shal'nov, K.V.: Phys. Solid State **43**, 878 (2001). doi:10.1134/1.1371369
14. Arbuzova, T.I., Naumov, S.V., Arbuzov, V.L., Shal'nov, K.V., Ermakov, A.E., Mysik, A.A.: Phys. Solid State **45**, 304 (2003). doi:10.1134/1.1553536
15. Petrov, M.I., Balaev, D.A., Shaikhutdinov, K.A., Ovchinnikov, S.G.: Phys. Solid State **40**, 1451 (1998). doi:10.1134/1.1130601
16. Forsyth, J.B., Brown, P.J., Wanklyn, B.M.: J. Phys. C **21**, 2917 (1988). doi:10.1088/0022-3719/21/15/023
17. Kondo, O., Ono, M., Sugiura, E., Sugiyama, K., Date, M.: J. Phys. Soc. Jpn. **57**, 3293 (1988). doi:10.1143/JPSJ.57.3293
18. Seehra, M.S., Dutta, P., Shim, H., Manivannan, A.: Solid State Commun. **129**, 721 (2004). doi:10.1016/j.ssc.2003.12.019
19. Zysler, R.D., Vasquez Mansilla, M., Fiorani, D.: Eur. Phys. J. B **41**, 171 (2004). doi:10.1140/epjb/e2004-00306-7
20. Liu, L., Hong, K., Hu, T., Xu, M.: J. Alloys Compd. **511**, 195 (2012). doi:10.1016/j.jallcom.2011.09.028
21. Srivastava, S., Kumar, M., Agrawal, A., Kumar Dwivedi, S.: J. Appl. Phys. (IOSR-JAP) **5**, 61 (2013)
22. Asharf Shah, M., Al-Ghamdi, M.S.: Mater. Sci. Appl. **2**, 977 (2011). doi:10.4236/msa.2011.28131
23. Swarnkar, R.K., Singh, S.C., Gopal, R.: Bull. Mater. Sci. **34**, 1363 (2011). doi:10.1007/s12034-011-0329-4
24. Musil, J., Baroch, P.: Vacuum **87**, 96 (2013). doi:10.1016/j.vacuum.2012.02.023
25. Nadeem, K., Krenn, H., Traußnig, T., Würschum, R., Szabó, D.V., Letofsky-Papst, I.: J. Appl. Phys. **111**, 113911 (2012). doi:10.1063/1.4724348
26. Synek, P., Jašek, O., Zajíčková, L.: Plasma Chem. Plasma Process. **34**, 327 (2014). doi:10.1007/s11090-014-9520-x
27. Lei, P., Boies, A., Calder, S., Girshick, S.: Plasma Chem. Plasma Process. **32**, 519 (2012). doi:10.1007/s11090-012-9364-1
28. Ushakov, A.V., Karpov, I.V., Lepeshev, A.A., Fedorov, L.Y.u., Shaikhadinov, A.A.: Tech. Phys. **86**, 103 (2016). doi:10.1134/S1063784216010230
29. Lepeshev, A.A., Karpov, I.V., Ushakov, A.V., Fedorov, L.Yu., Shaikhadinov, A.A.: Int. J. Nanosci. **15**, 1550027 (2016). doi:10.1142/S0219581X15500271
30. Ushakov, A.V., Karpov, I.V., Lepeshev, A.A., Zharkov, S.M.: Vacuum **128**, 123 (2016). doi:10.1016/j.vacuum.2016.03.025
31. Fedorov, L.Y.u., Karpov, I.V., Ushakov, A.V., Lepeshev, A.A.: Inorg. Mater. **51**, 25 (2015). doi:10.1134/S0020168515010057
32. Ushakov, A.V., Karpov, I.V., Lepeshev, A.A.: Tech. Phys. **86**, 260 (2016). doi:10.1134/S1063784216020262
33. Ushakov, A.V., Karpov, I.V., Lepeshev, A.A.: Phys. Solid State **57**, 2320 (2015). doi:10.1134/S1063783415110359
34. Ushakov, A.V., Karpov, I.V., Lepeshev, A.A., Petrov, M.I.: J. Appl. Phys. **118**, 023907 (2015). doi:10.1063/1.4926549
35. Ushakov, A.V., Karpov, I.V., Lepeshev, A.A., Petrov, M.I., Fedorov, L.Y.u.: Phys. Solid State **57**, 919 (2015). doi:10.1134/S1063783415050303
36. Ushakov, A.V., Karpov, I.V., Lepeshev, A.A., Petorv, M.I., Fedorov, L.Y.U.: JETP Lett. **99**, 99 (2014). doi:10.1134/S002136401402009X
37. Karpov, I.V., Ushakov, A.V., Fedorov, L.Y.u., Lepeshev, A.A.: Tech. Phys. **84**, 559 (2014). doi:10.1134/S1063784214040148
38. Rietveld, H.M.: J. Appl. Crystallogr. **2**, 65 (1969). doi:10.1107/S0021889869006